Electronic Supplementary Material (ESI) for Green Chemistry.

Interfacial improvements in biocomposites based on poly(3-hydroxybutyrate) and poly(3-hydroxybutyrate-*co*-3-hydroxyvalerate) bioplastics reinforced and grafted with *α*-cellulose fibers

Liqing Wei [a], Nicole M. Stark [b], and Armando G. McDonald [a,*]

[a] Renewable Materials Program, Department of Forest, Rangeland and Fire Sciences, University of Idaho, Moscow, Idaho 83844-1132, United States

[b] U.S. Department of Agriculture, Forest Service, Forest Products Laboratory, One Gifford Pinchot Drive, Madison, Wisconsin 53726-2398, United States

[*] Corresponding author. Tel.: +1 (208) 885 9454; Fax: +1 (208) 885 6226; E-mail address: armandm@uidaho.edu

Table of contents

This in-situ grafting modification offers an effective approach to improve the properties of biocomposite materials from sustainable resources.

Abstract

In this study, α-cellulose fibers reinforced green biocomposites based on polyhydroxybutyrate (PHB) and the copolymer poly(3-hydroxybutyrate-*co*-3-hydroxyvalerate) (PHBV) were prepared and characterized. The α-cellulose fibers were isolated from at-risk intermountain lodgepole pine wood by successive removing of extractives, lignin and hemicellulose. Grafting of PHB or PHBV onto cellulose was conducted using reactive extrusion with dicumyl peroxide free radical initiation at high temperature. It is postulated that the grafted copolymers at the interfaces of cellulose and polymer matrix performed as interfacial coupling agent. Grafting tended to interact with both the hydrophilic fibers and hydrophobic PHB or PHBV matrix. The biocomposites were characterized by scanning electron microscopy (SEM) and dynamic mechanical analysis (DMA) and indicated good interfacial bonding and compatibility between the two phases. The mechanical properties of the biocomposites were improved by grafting due to improved stress transfer between the two interphases of fiber/polymer matrix as compared to the blend control composite. The crystallinity of PHB, PHBV and cellulose in the biocomposite were reduced as determined by Fourier transform infrared spectroscopy (FTIR), wide-angle X-ray diffraction (WAXD), and differential scanning calorimetry (DSC) analyses. This *in-situ* reactive extrusion process offers an effective approach to improve the properties of biocomposite materials from sustainable resources.

1. Introduction

Strong, lightweight, and moldable plastics are used in thousands of products that improve the quality and bring convenience to our everyday lives. However, at least 40% of these conventional (petroleum-based) plastics are used in short-term applications (e.g. throwaway

cups, utensils, plastic bags) and after being disposed the resulting waste can quickly lead to both terrestrial and marine environmental pollution.[1, 2] In brief, petroleum-based plastics are not sustainable, which drives the efforts to develop more environmentally benign plastics and materials. Some of the most commonly known bio-based and biodegradable plastics from renewable resources include polylactic acid (PLA), polyhydroxyalkanoates [PHAs, e.g. polyhydroxybutyrate (PHB) and poly(hdyroxybutyrate-co-hydroxyvalerate) (PHBV)], thermoplastic starch, protein based plastics and the most abundant terrestial polymer on earth, cellulose and its derivatives.[3, 4] Extensive application of these bioplastics, notably PHB and PHBV, will occur only after overcoming challenges including poor melt elasticity, low thermal degradation temperature, high crystallinity leading to brittleness for PHB, and low crystallization rate of PHBV.[5, 6] These features, especially low melt elasticity, limit their processibility window, for example, during extrusion processes typically used for film, injection molding, blown-film manufacture, thermoforming, and fiber spinning.[5, 7]

Another critical issue is the millions of acres of forestland that have become prone to disease and insect attack in the Inland-Northwest of the United State, and high risk for catastrophic wildfire because of overstocked stands.[8] Approximately 6 million dry tons of sound dead wood from Idaho's National Forests is available. Of this, a sustainable level of over one million dry tons/year of logging residues and thinnings are potentially available for producing a variety of bioproducts. Therefore, there is a need to generate materials, such as cellulose, from this abundant woody biomass for use in value-added products.

Wood fibers have been used as fillers in thermoplastics to produce wood plastic composites (WPCs), which can be used in various applications (decks, railings and automotive) due to their well acceptable properties, low costs, and renewability.[9] WPC performances can be further

improved by exchanging wood fiber for cellulose fiber based on its improved thermal stability and mechanical properties. The cellulose fibers have been widely used as reinforcing filler into conventional thermoplastics, such as polypropylene and polyethylene.[10-13] Some mechanical properties, such as Young's modulus and tensile strength, were improved due to the addition of cellulose fibers.[12] However, the presence of a large number of hydroxyl groups results in a polar fiber surface; it is very difficult to disperse polar cellulose in a non-polar polymer matrix. This difficulty can result in poor interfacial bonding between the cellulose and thepolymer matrix. Poor adhesion at the interface means that the full capabilities of the composite cannot be exploited and leads to low mechanical properties and a reduced life span.[11] Due to this reason, cellulose performs as simple filler not a true reinforcing agent. Research to improve the interfacial adhesion of biocomposites continues. Extensive studies have been conducted using coupling agents (e.g. maleated-polypropylene and maleated-polyethylene) to enhance the interfacial adhesion of fiber filler and polymer matrix.[14] Other efforts including chemical/physical treatments of fiber fillers to reduce the hydrophilicity of cellulose fiber surfaces have gained much more attention.[15-18] Although these modifications result in a decrease in moisture absorption and an increase in mechanical properties, biodurability and weatherability, the processes used for cellulose modification are costly and involve toxic chemicals which could be a deterrent to its use.[9, 19]

By exchanging conventional plastics (e.g. polyethylene and polypropylene) with bioplastics (e.g. PHB and PHBV), which are less hydrophobic, will produce a fully bio-based composite material that is sustainably derived with good mechanical properties (flexural/tensile strength and stiffness) and biodegradation behaviors.[17, 20-22] Additionally, biocomposite properties can be improved by incorporating modified cellulose fibers into a bioplastic matrix.[23-25] Recently, the

reaction mechanism of a "grafting onto" method has been successfully studied by grafting PHB polymer onto cellulose fibers through the reactive extrusion processing with the use of small amount of peroxide (Fig. 1).[26] When the peroxide is exposed to heat during extrusion it will decompose into strong free radicals which tend to abstract H's from the polymer and cellulose molecular chains and initiate the grafting between the two phases in composites. Via the strategy of grafting PHB or PHBV onto cellulose this will retain the stiffness of cellulose and the flexibility of the polymer matrix (PHBV especially). In addition, the use of reactive extrusion which limits the use of solvents and the treatment of cellulose, which makes it a valuable alternative to improve the performances of cellulose reinforced bioplastics composites. Chemically coupling PHB to cellulose fiber provides excellent stress transfer and hydrophobic-hydrophilic compatibility between the two phases in the biocomposite material with no external non-biodegradable coupling agent or compatibilizers are employed. This in-line modification process can be applied easily to industrial scale production of biocomposites.

Our aim in this study was to isolate *α*-cellulose (*α*Cell) fibers from in-risk lodgepole pine wood. The "grafting onto" strategy was used to prepare cellulose-graft-PHBV (*α*Cell-*g*-PHBV) or *α*Cell-*g*-PHB biocomposites with improved properties due to enhanced interfacial adhesion. The surface morphology, chemistry, and crystalline structure of the modified biocomposites were characterized by microscopy, Fourier transform infrared spectroscopy (FTIR) spectroscopy, and wide angle X-ray diffraction (WAXD), respectively. Tensile tests were conducted on the injection molded dog-bone specimens. Thermal properties, such as thermal transition and crystallinity, thermal degradation, dynamic flexural properties, and thermal mechanical properties of biocomposites were assessed by thermal analysis.

2. Results and discussion

2.1. *α*-Cellulose fiber analysis

The chemical composition of the original wood and *α*Cell fibers for CH_2Cl_2 extractive, lignin, and carbohydrate content/composition was determined and shown in Table 1.[27] Lodgepole pine wood was comprised of 39% cellulose. After isolation, *α*Cell had a 96% purity based on glucose content.

The *α*Cell fiber size (weight) distribution was determined using an automatic vibratory sieve shaker. As shown in Table 2, the major part of the *α*Cell fiber was smaller than 250 μm, with 65% of the fibers were between 70 and 177 μm. Further information concerning *α*Cell fiber size (length and diameter) was achieved by optical microscopy. The micrographs of each screened fraction are shown in Fig. 2. Single fibers were observed (rod like), especially for the fractions that were > 60 mesh (Fig. 2c, 2d, 2e and 2f). The length (L) and diameter (d) of these fibers fractions were measured and averaged from 200 fibers. The weight normalized fiber L and d were 0.5 mm and 15.1 μm, respectively. The L of the >80, >100, and >200 mesh classified fibers ranged between 0.6 and 0.8 mm, while the d of these fractions were comparable around 19 μm. The fines fraction (<200 mesh) had a much smaller L (0.4 mm) and d (14 μm) than the coarser fractions. The 40 and 60 mesh fractions comprised of fiber bundles (Fig. 2a and 2b); hence the fiber length and diameter were difficult to be determined. As shown in Table 2, 59% (weight fraction) of the *α*Cell fibers had an aspect ratio (L/d) of 31 and is considered microcrystalline.[28] The aspect ratio was shown to decrease with a finer mesh size.

2.2. Reaction conditions optimization and grafting efficiency

The effect of two factors (DCP concentration: 2-5 %; reaction time, t_R: 5-15 min) was

investigated to optimize the grafting efficiency between *α*Cell and PHB (or PHBV) polymer matrix. The extruded composite strands were extracted with $CHCl_3$ to remove any nonreacted PHB/PHBV or smaller homopolymer molecules and then filtered to remove nongrafted *α*Cell fibers (Note: CH_2Cl_2 and $CHCl_3$ used in this research were recovered for reuse to reduce environmental impact). The dry weight of the copolymer gels was recorded and gel% was calculated with respect to the dry weight of the starting materials. The optimized total concentration of DCP and t_R were 2% and 10 min, respectively, to give the maximum *α*Cell-*g*-PHB and *α*Cell-*g*-PHBV copolymer gel% and well mixed biocomposites samples. The degree of grafting efficiency (GE%, weight % of PHBV (or PHB)) grafted onto *α*Cell backbone was calculated),

$$GE\% = (W_{gf} - W_{\alpha Cell})/W_{PHB/PHBV} \times 100 \qquad (1)$$

where W_{gf}, $W_{\alpha Cell}$, and $W_{PHB/PHBV}$ are the weights of the grafted copolymer gel recovered after Soxhlet extraction, initial *α*Cell, and initial PHB (or PHBV) weights, respectively.[19] The simple blended composites were also extracted in the same way as grafted samples. The GE% of simple blends was < 0.5%, and thus being neglected in this study. The highest GE% value of *α*Cell with PHBV was 45% but that with PHB was 35%, when biocomposites were processed under the same optimized reactive conditions (DCP: 2 wt%; t_R: 10 min). As shown in Fig. 1, the grafting reactions occurred at the tertiary –CH sites of PHB and PHBV. PHBV copolymer has one additional tertiary –CH site in each comonomeric unit as compared with the PHB, therefore, higher GE% was observed for *α*Cell-*g*-PHBV copolymers. It is worth noting that the high GE% can also be ascribed to partial crosslinking/grafting of the polymer matrices (Fig. 1a).

2.3. Surface morphology of biocomposites

154 The SEM micrographs of the biocomposites surfaces are shown in Fig. 3. The grafted
155 biocomposites (Fig. 3b and 3d) showed a continuous interphase between fiber and polymer
156 matrix, indicating that the polymer was grafted onto *α*Cell by peroxide initiation. In contrast,
157 blends of *α*Cell-PHB and *α*Cell-PHBV showed discrete zones of PHB or PHBV and *α*Cell fibers
158 (Fig. 3a and 3c), and the fibers were easily pulled out from the matrix when microtomed. A
159 similar trend was observed with peroxide treated sisal fibers filled in polyethylene composites
160 system.[29] An improved compatibility between *α*Cell and the polymer matrix was obtained due to
161 peroxide induced grafting (Fig. 3b and 3d)**.** It was therefore postulated that the grafted copolymer
162 formed on the interfaces of *α*Cell and PHBV (or PHB) coupled the hydrophilic *α*Cell to the
163 hydrophobic PHBV (or PHB) matrix (Fig. 1). Micrographs at magnification of 200x (Fig. 3e to
164 3h) showed the cellulose fibers have been separated during the mixing extrusion process are well
165 dispersed in the polymer matrices, especially in the grafted composites as compared to the
166 simple blends. On average a random orientation of cellulose fibers into the polymer matrices for
167 both grafting as well as their simple blends was observed. However, the surfaces of *α*Cell fibers
168 became rougher and more amorphous due to peroxide treatment, which may provide higher
169 possibility of access for melted polymers to attach onto during composites processing. This
170 further suggested better interfacial adhesion between *α*Cell fibers and PHB (or PHBV) due to
171 grafting.
172
173 **2.4. Characterization of biocomposites by FTIR and XRD**
174 The crystalline nature of PHB and its composites materials significantly affect their
175 mechanical properties and processability as well. Copolymerization of 3-hydroxybutyrate with
176 other monomeric units, such as 3-hydroxyvalerate (3HV), to form PHBV copolymers has been

proven to be one of the most effective strategies to reduce the crystallinity of PHB. These copolymers showed improved mechanical properties as a result of being less crystalline, which is contributed to the presence of dislocations, crystal strain and smaller crystallite sizes due to the disruption of 3HV unit to PHB crystal lattice.[30] The degree of crystallinity of PHB and PHBV can be obtained by a combination of FTIR and WAXD analyses. Fig. 4a showed the FTIR spectrum of the composites samples with characteristic absorbance peaks arising from *α*Cell and PHBV (or PHB). The absorbance bands at 980, 1230, 1720 cm^{-1} were assigned to the crystalline regions of PHB or PHBV polymers, and as expected the intensities of these peaks were lower for PHBV based samples than those of PHB's. This further indicated that the copolymer PHBV was less crystalline than PHB. It was shown that the intensities of these crystalline bands for the grafted composites were reduced significantly, due to grafting, compared to their simple blends (*α*Cell-PHB and *α*Cell-PHBV). The shoulder at 1740 cm^{-1} of the band centered at 1720 cm^{-1} was assigned to the carbonyl (C=O stretching) group from the amorphous region of PHB and PHBV, and it became more intense after grafting (see the peak fitting of C=O region showing in Fig. 4c). This observation suggested that successful grafting between the matrix (PHB and PHBV) and *α*Cell reinforcement was achieved, which would hinder the crystallization of PHBV (or PHB) macromolecular chains from melts, resulting in a higher proportion of amorphous PHBV (or PHB). It is worth noting that the reduction of crystallinity of grafted composites could also be attributed to the crosslinking of polymer matrix (PHB-PHB or PHBV-PHBV). In addition, due to the high degree of crystallinity/rigidity with the less mobile cellulose, only radicals formed on its surfaces of the crystalline and amorphous regions would be more accessible to the molten PHB/PHBV (with radicals) which would then be able to form grafts in the composites. Therefore, the band at 1429 cm^{-1} (symmetric $–CH_2$ bending), a characteristic of amorphous

cellulose, which appeared in the grafted composites, again providing further evidence that grafting had occurred. To further confirm that the crystallinity was reduced due to grafting, quantitative analyses of the spectra for PHBV (and PHB) and cellulose crystallinity were performed. The spectral ratio of 1370/2900 cm^{-1} bands (total crystallinity index, TCI, Equation 3) was shown to be proportional to the crystallinity degree of cellulose, while the band ratios 1720/1740 cm^{-1} (carbonyl index, $I_{C=O,PHB/PHBV}$, Equation 4) and 1230/1450 cm^{-1} (C-O index, $I_{C-O,PHB/PHBV}$, Equation 5) reflect the crystallinity of PHB or PHBV polymers. Quantitative analysis of the infrared crystallinity ratios were calculated from the peak fitted spectra of the –C–H (and –CH_2 stretching) at 2900 cm^{-1} (Fig. 4b), the carbonyl region (1800-1680 cm^{-1}) for PHB (Fig. 4c), and –C–H bending centered and1370 cm^{-1} from crystalline region for cellulose (Fig. 4d). The analyzed data for neat PHB and PHBV, *α*Cell, *α*Cell-PHB blend, *α*Cell-PHBV blend, and grafted composites (*α*Cell-*g*-PHB and *α*Cell-*g*-PHBV) are given in Table 4. The addition of αCell resulted in a reduction in PHBV (and PHB) crystallinity of the blended composites slightly, while grafting reduced all the three crystallinity indices significantly. The grafted copolymers between αCell and PHBV (or PHB) matrix had improved compatibility, which would improve the stress transfer between the two phases of hydrophilic cellulose and hydrophobic polymer.[26]

To further investigate the effect of the grafting on the crystalline structures of PHB and cellulose segments, vacuum dried samples were subjected to WAXD analysis (Fig. 5). *α*Cell showed four crystalline peaks corresponding to (101), (10-1), (002), and (040) planes showing at 2θ scale of 14°, 16°, 22°, and 35°, respectively. The maximum diffractogram intensity was observed in the (002) plane. This is a typical pattern of cellulose I. Both PHB and PHBV samples showed crystalline peaks at 2θ near to 13°, 17°, 20°, 21°, 22°, 26° and 27°, respectively, ascribing to planes of (020), (110), (021), (101), (121), (040), and (200). The most intense peak

for PHB and the composites samples was at 17°, whereas the most intense peak for PHBV based samples was observed at 13°. It is assumed that the reduced crystallinity of PHBV as compared to PHB could be the main contributor to peak broadening for all the crystalline planes. Such results can be explained by the reason that the presence of *α*Cell suppressed the nucleation of polymer, especially for PHBV, in the simple blends. The similar reduction of PHB and PHBV crystallinity was also found in PHB/cellulose (Whatman CF1) and PHBV/PLA/PBS (poly(butylene succinate)) blends, respectively.[26]

The Gaussian function was used for peak fitting of the WAXD diffractograms, meantime, the FWHM values were obtained accordingly. Crystallinity indices were calculated from the ratios of fitted peak intensities, and crystal sizes according to Scherrer's formula using a shape constant K = 0.9 for PHBV (and PHB) and cellulose (Table 3). Crystallinity index[19] and average crystal width were 59.1% ($CrI\%_{\alpha Cell}$, Equation 6) and 250 Å (D_{002}) for *α*Cell, 61% ($CrI\%_{PHB}$, Equation 7) and 1274 Å (D_{020}) for PHB, and 36.2% ($CrI\%_{PHBV}$, Equation 8) and 190 Å (D_{020}, Equation 9) for PHBV, respectively. PHBV had a much smaller crystal size and significantly lower degree of crystallinity than PHB based materials. The lower crystallinity for PHBV would result in a more ductile/flexible material than PHB. The large crystal size which would induce inter-spherulitic cracks is one of the leading reasons for the brittleness of PHB.[31, 32] The simple blending of PHB (or PHBV) with *α*Cell was shown to reduce slightly the crystallinity indices and crystal sizes of the PHB (or PHBV) polymer. Nevertheless, the decreasing trend was more significant as a result of grafting (Table 3), which contributed to new C–C bonds being formed which limited the numbers of PHB or PHBV molecular chains involved in crystallization processes from the polymer melt. The PHB and PHBV molecular chains with more grafted sites would contribute to an increase in the amorphous component due to inhibited crystallization.

These results were consistent with the findings from infrared crystallinity indices results and supported the lowering in crystallinity of the polymer matrix by grafting. Smaller crystal sizes of the grafted biocomposites were observed suggesting that the formation of large crystals of either PHBV (or PHB) was restricted. This could be one of the major reasons for to the improved mechanical properties of grafted biocomposites as compared to the simple blends of cellulose and polymer (PHB or PHBV).

2.5. Influence of grafting on mechanical properties of biocomposites

The density (ρ) and tensile properties (strength (σ), modulus (E), elongation at break (ε), and energy at break (EAB)) of molded neat bioplastics and their composites are given in Table 4. The ρ of all PHB, PHBV and biocomposites samples ranged from 1.10 to 1.18 g/cm^3 and thus was not a major factor causing differences in tensile properties between treatments. The density of the biocomposites remains similar to neat plastics, which may be because the density of cellulose fiber was about 1.5 g/cm^3 and only 20% of cellulose was used in the composites.

According to Maldas and Kokta,[33] the mechanical properties of short-fibers and plastic composites are strongly influenced by the fiber content, fiber morphology (size and shape), the orientation (random or unidirectional) of the fillers, and the fiber-polymer adhesion. The σ is more dependent on the fiber-polymer interaction (compatibility) while E is dependent more on fiber content and morphology (i.e. aspect ratio).[14] The grafted biocomposites resulted in an increase of E and σ. The E values of αCell-PHB and αCell-PHBV biocomposites were higher than those of the neat PHB and PHBV, respectively. This indicated the reinforcement effect of cellulose fibers to the polymer matrices. On the other hand, the increments of E were much more significantly for the grafted composites due to grafting between cellulose and polymer matrices.

The neat PHBV and blended *α*Cell-PHBV composite showed lower *E* as compared to PHB and blended *α*Cell-PHB, which was attributed to the lower tensile properties of PHBV.[34] Whereas, the grafted *α*Cell-*g*-PHBV composites showed comparable *E* to neat PHB, suggesting the reinforcement of *α*Cell fibers was improved via grafting. Moreover, the increased *E* of polymer matrix due to crosslinking between polymer chains (see Fig. 1) would partially contribute to the *E* increase of grafted composites.

The ductility reflected by *ε* values was significantly higher for PHBV based composites, which contributed to higher flexibility of PHBV (22% HV) than PHB homopolymers.[32] Work on PHB/PHBV-flax fiber composites showed higher values of *ε* for PHBV based composites than PHB based composites.[34] For composites made from PHB or PHBV, *σ* at ultimate yield point was increased with the addition of *α*Cell fibers accompanied with a decrease in *ε*. In comparison with PHB and its composites the copolymer PHBV based composites showed a somewhat lower *σ*, around 12 MPa. For the grafted composites (*α*Cell-*g*-PHB and *α*Cell-*g*-PHBV), higher *E* and *ε* were obtained when compared to their simple blends. This finding suggests that grafting didn't just enhance the fiber-polymer matrix interaction but also increased the ductility of the resulting composite due to crosslinking between polymer chains (PHB-PHB and PHBV-PHBV). This was possibly caused by a lower degree of crystallinity of cellulose and the bioplastic as discussed in the previous section (Table 3). The toughness of all samples was assessed by their EAB values (Table 4). Neat PHB and PHBV showed respective toughness of 0.33 and 0.45 J, indicating that the PHBV copolymers had an improved toughness than PHB. EAB was also shown to increase with addition of 20% *α*Cell fibers. For example, the EAB of the simple blends, *α*Cell-PHB and *α*Cell-PHBV, were 0.41 and 0.45 J, respectively. A similar result was obtained in a study on the fracture toughness changes due to addition of 10 to 30 % wheat straw fibers into PHB matrix.[35]

Grafting of PHB/PHBV onto *α*Cell improved the toughness significantly ($p < 0.05$) by 46% and 44%, respectively, as compared to their simple blends, *α*Cell-PHB and *α*Cell-PHBV.

According to Kelly-Tyson theory, the critical fiber length ($L_{c/\alpha Cell}$) is used to evaluate the fibers performing as reinforcement or just filler to the polymer matrix. It is assumed fiber morphology (length and aspect ratio) would not be influenced significantly during single screw mixing/extrusion processing, for example by shearing, and thus the $L_{c/\alpha Cell}$ can be estimated as follows:

$$L_{c/\alpha Cell} = \frac{\sigma_{\alpha Cell} \times d_{\alpha Cell}}{2\tau} \quad (2)$$

where $\sigma_{\alpha Cell}$ is the *α*Cell fiber strength, $d_{\alpha Cell}$ is the fiber diameter that was averaged based on the weight fraction % ($d_{\alpha Cell}$ = 0.015 mm), and τ is the interfacial bonding strength of fiber and polymer matrix. $\sigma_{\alpha Cell}$ and τ values were obtained from the literature, respectively at 1.5 GPa and 8.8 MPa.[34] Hence, the $L_{c/\alpha Cell}$ value was calculated to be 1.2 mm. Based on the fiber distribution analysis as shown in Table 2, the size of *α*Cell fibers were lower than the estimated critical length required to give an adequate stress transfer between fiber and PHB (or PHBV) polymer matrix. This again explained the low σ of simple blended composites without grafting. However, the grafted composites (*α*Cell-*g*-PHB and *α*Cell-*g*-PHBV) showed improved tensile properties due to better stress transfer caused by the newly formed bonds (Fig. 1) between the fiber and polymer.

2.6. Thermal properties of the bioplastics and biocomposites

2.6.1. Thermal degradation behavior

Thermal degradation for neat PHB and PHBV and biocomposites was investigated by thermogravimetric analysis (TGA) and the degradation temperatures are given in Table 5. Neat

315 PHB and PHBV started (T_{onset}) to degrade at 263 and 250 ˚C, and completed degradation (T_{comp})
316 at 303 and 292 ˚C, respectively. The HV units in PHBV did not improve the thermal stability of
317 the polymer, which agrees to previous research.[36] Degradation (98% mass loss) occurred in one
318 step for the neat polymers. This was ascribed to chain scission and hydrolysis mechanisms of
319 PHB and PHBV, resulting in a lower molar mass fragments and the formation of crotonic acid.[36]
320 All the biocomposite samples showed two degradation stages, of which the first stage was
321 ascribed to the PHB/PHBV degradation while the second stage was from *α*Cell degradation. The
322 T_{onset} for the *α*Cell-PHB and *α*Cell-PHBV blends was close to neat PHB/PHBV, and 80% of the
323 biocomposite samples degraded in the first stage, aligning to the formulation (*α*Cell:PHB = 1:4;
324 *α*Cell:PHBV = 1:4). These data indicated that simple blending of *α*Cell fibers with PHB/PHBV
325 did not improve the thermal stability of the polymer matrix. These results are consistent with
326 findings for PHB and cotton fiber blends.[26] However, the grafted biocomposites (*α*Cell-*g*-PHB
327 and *α*Cell-*g*-PHBV) had a higher T_{onset} by > 10 ˚C than neat PHB and PHBV. The temperature of
328 maximum decomposition rate (T_{max}) in the first stage for sample *α*Cell-*g*-PHB was > 10 ˚C
329 higher than T_{max} of neat PHB (285 ˚C). Furthermore, the T_{max} in the second stage due to *α*Cell
330 ($T_{\alpha Cell}$) component degradation was also increased compared to *α*Cell-PHB blends. Similar
331 results were obtained for PHBV based biocomposites. Grafting modification improved the
332 thermal stability for both the reinforcement (*α*Cell) and the polymer matrix (PHB and PHBV).
333 Grafting between *α*Cell and polymer matrix and a small amount of cross-linked PHB or PHBV
334 resulted in forming more C–C bonds (Fig. 1b and 1c), which would require more energy/thermal
335 input to decompose the resultant grafted biocomposites.
336
337 2.6.2. Different scanning calorimetry (DSC) analysis

338 The thermal events of glass, crystallization, melting transitions of neat PHB/PHBV, simple
339 blends, and grafted biocomposites were studied using DSC. Fig. 6 shows the DSC thermograms
340 for neat PHB and PHBV, and their biocomposites in the temperature range of -30 to 180 ˚C.
341 Thermal transitions as well as the degree of crystallinity (X_c %, Equation 10) of the materials are
342 given in Table 6. Neat PHB showed a glass transition (T_g = 4.9 ˚C) and double endothermic
343 peaks (T_{m1} = 159 ˚C and T_{m2} = 169 ˚C, labeled from low to high temperatures) corresponding to
344 melting points in the second heating scan (Fig. 6). The addition of 20 wt% *α*Cell to neat PHB
345 (*α*Cell-PHB blend) resulted in a slight increase in T_g (5.3 ˚C), while the grafted *α*Cell-*g*-PHB
346 biocomposites increased T_g by 2 ˚C. The X_c % of *α*Cell-PHB and *α*Cell-*g*-PHB biocomposites
347 was reduced by 2.4 % and 10.4 %, respectively, as compared to neat PHB (53.4%). The
348 reduction in crystallinity (or amorphous phase increase) observed by DSC agreed with results of
349 FTIR and WAXD analyses (Table 4).
350 The T_g is directly associated with the macromolecular mobility of polymer chains, hence, a
351 lower X_c % will require less energy to move the polymer chains in the amorphous phase.
352 Therefore, a lower T_g is expected to transit the polymer from a glassy to a rubbery state if only
353 polymer matrix itself was modified by DCP as reported in our previous studies.[37] However,
354 higher T_g was observed for *α*Cell-PHB and *α*Cell-*g*-PHB biocomposites, which was possibly due
355 to the limited polymer molecular chain mobility from the rigid *α*Cell fibers. Bhardwaj et al.[38]
356 found the similar trend for T_g of recycled fibers reinforced PHBV composites. In *α*Cell-*g*-PHB,
357 extra C–C bonds due to grafting between the fibers and polymer matrix would provide further
358 restrictions in the polymer chain mobility as compared to *α*Cell-PHB, and hence T_g was shifted
359 to a higher temperature.
360 During DSC analysis, the melt peaks, T_{m1} and $T_{m2,}$ of *α*Cell-PHB were increased slightly

from 159 to 161 ˚C and from 169 to 171 ˚C, respectively, as compared to neat PHB. While the *α*Cell-*g*-PHB composites showed T_{m1} and T_{m2} values respectively at 155 and 164 ˚C. This reduction is likely caused by the broadening molar mass distribution of the polymer matrix due to grafting/cross-linking between polymer chains. A similar trend was observed for T_g, T_m's and X_c % for PHBV and its biocomposites samples (Table 6). However, a more apparent change was seen in the grafted *α*Cell-*g*-PHBV material. This could be contributed to the chemical structure of PHBV/PHB polymers[26] and the higher GE% of PHBV.

DSC can easily detect the significant heat release accompanying the exothermic crystallization process of PHB and PHBV. The T_c is an important thermal parameter to describe the crystallization behavior of fiber and plastic composites (Fig. 6 and Table 6). A sharp crystallization peak was observed for all PHB-based samples and neat PHBV in the cooling scan. An increase in T_c was observed when *α*Cell fibers were incorporated into the PHB matrix (T_c = 85 ˚C). This suggested that the *α*Cell fibers induced nucleation of PHB and initiated the crystallization at higher temperature (i.e. > 121 ˚C) from melt. Grafting resulted in a decrease in T_c (103 ˚C) of *α*Cell-*g*-PHB as compared to the blended *α*Cell-PHB material. The corresponding enthalpy (ΔH_c) of *α*Cell-*g*-PHB during crystallization was reduced by 12 % due to grafting. This reduction was most likely due to the lower X_c % of PHBV (or PHB) in the grafted biocomposites (Table 6). The exothermic peak of neat PHBV was broader than PHB, which indicated nucleation and crystal growth were much slower in PHBV. This finding agrees with the literature.[39] The T_c of PHBV in *α*Cell-PHBV was reduced significantly by 28 ˚C as compared to that of neat PHBV. This indicated that the addition of fibers resulted in a slower diffusion and migration of PHBV copolymer chains to the surface of the nucleation point, thus decreasing T_c during cooling of the *α*Cell-PHBV melt. For the grafted biocomposites, *α*Cell-*g*-PHBV, no

384 exothermic crystallization peak (T_c) was observed by DSC in the cooling scan. The reduction in
385 the X_c %, T_m's, and T_c was in agreement with the results reported in the case of poly(ε-
386 caprolactone) (PCL) reinforced with PCL diol grafted cellulose nanocrystals using toluene 2,4-
387 diisocyanate as coupling agent.[40] In addition, an exothermal (cold crystallization) peak (T_{cc}) was
388 observed in the heating scan of PHBV based composites (Fig. 6b). This peak was shifted from 56
389 ˚C to higher temperature (77 ˚C) due to grafting, indicating the delay of crystallization kinetics
390 (increased crystallization rate) with incorporation of cellulose fibers and grafting crosslinks.
391
392 2.6.3. Dynamic flexural properties
393 Dynamic mechanical analysis (DMA) was performed on PHB, PHBV and their composites
394 in three-point bending mode to determine the storage modulus (*E*') which determines the
395 dynamic rigidity of a material. The *E*' values of the samples at 30, 50 and 70 ˚C are given in
396 Table 7. The *E*' values (30 ˚C) of PHB increased by 33% and 60%, respectively by simple
397 addition of *α*Cell and grafting of *α*Cell, respectively. The *α*Cell-PHBV and *α*Cell-*g*-PHBV
398 biocomposites had also shown significantly increased *E*' values by 88 and 127%, respectively, as
399 compared to neat PHBV. PHB had a higher *E*' due to its high brittleness than PHBV. The higher
400 *E*' values for the grafted composites could be contributed to an improved compatibility and
401 dispersion of *α*Cell fibers in the PHB/PHBV matrix as compared to their blends (*α*Cell-PHB and
402 *α*Cell-PHBV). Better stress transfer between the *α*Cell and PHB/PHBV interfaces of the grafted
403 composites would also improve the rigidity of either PHB or PHBV composites.
404 The loss tangents (tan*δ*) of the various samples at 30, 50 and 70 ˚C are given in Table 7 as
405 well. Tan*δ* values were shown to have a minimum at 50 ˚C. For both PHB and PHBV based
406 composites their tan*δ* values were less than their matrix, especially < 30 ˚C. According to our

previous findings of the fiber-matrix interfacial bonding,[9, 25] the reduction of tanδ could indicate better interfacial adhesion of these two phases in grafted biocomposites as compared to their simple blends without being grafting modified.

The interfacial bonding between wood fiber and polyethylene matrix was successfully evaluated by the adhesion factor (A) (Equation 11).[9] A values derived from DMA data at 30 ˚C are given in Table 7. Lower A values of the grafted composites was an indicator of improved interfacial interaction between the two phases, αCell and PHB or PHBV, as compared to their blend. These data provided supportive evidence that an improved interaction was achieved by grafting.

2.7. Dynamic rheological properties

The polymer melt properties of the biocomposites were determined by dynamic parallel plate rheometry. Fig. 7 shows the dynamic elastics and viscous moduli (G' and G") of PHB (175 ˚C) and PHBV (170 ˚C) based materials under isothermal conditions. For the PHB based composites both G' and G" were shown to increase with frequency (ω, rad/s). At lower ω, G" was higher than G' for PHB and the simple blended composite (αCell-PHB). This indicated that these samples were more liquid-like, although the incorporation of αCell made the resulting composites slightly more elastic which was reflected by the less difference between G" and G' values. However, grafting improved the G' slightly compared to the simple blends (see Fig. 7a, G' > G"), suggesting the grafted PHB onto αCell showed good elastic properties. For instance, G' was increased from 12 Pa (PHB) to 1000 Pa by addition of αCell and further improvement to 1400 Pa was obtained by grafting (αCell-*g*-PHB). PHBV, αCell-PHBV and αCell-*g*-PHBV showed higher G' and G" values than PHB series which clearly showed that the PHBV

copolymer had relatively better melt strength. At lower frequency, i. e. $\omega < 10$ rad/s, G' > G" was observed for PHBV and its composites, suggesting the PHBV (22 mol% HV) has better melt strength (higher melt viscosity) than PHB. Conflicting results were observed in other studies on the PHBV with lower HV content (12 mol%).[41] In addition, due to relatively longer chain of HV as compared to HB more degrees of chain entanglements in PHBV would be presented as compared to PHB. Found in previous researches,[37, 42] the melt elasticity is positively proportional to the molecular chain entanglement and the degree of long chain branching. Although pure PHBV is a linear polymer, the presence of HV monomeric units could provide long chain branching structures. Compared to pure PHB homopolymers, PHBV can be considered as a branched form of PHB, and thus PHBV and its composites showed G' > G". Similar trend (G' > G") was observed between the long chain branched and linear polyethylene samples.[42]

The polymer melt of the copolymer PHBV had better elasticity than that of PHB (Fig. 7b). The addition of *α*Cell to PHBV increased its G" by 30%. The effect of grafting of *α*Cell onto PHBV further increased G' (5-fold) and G" (7-fold) significantly as compared to the blend. The improvements of PHBV properties, relative to PHB, are most likely due to the higher grafting efficiency of PHBV when using the same reactive parameters.

The cross-over modulus (G_c = G' = G") of grafted PHB and PHBV biocomposites shifted towards higher ω. The G_c was increased from 670 Pa for PHB to 1070 Pa by addition of *α*Cell and was further increased to 2300 Pa by grafting. A similar trend was also observed for the PHBV composite series. The mean relaxation time (at G_c), which is the ratio of the elastic to the viscous response,[43] was increased for PHB based composites whereas it was decreased for PHBV based composites due to grafting. This difference might be mainly due to the higher molecular weight of PHBV as well as the fraction of crosslinked polymer (PHB-PHB,

PHBV/PHBV) in the grafted composites. This can result in higher molar mass distribution of grafted PHBV based composites than that of PHB based composites.

*α*Cell-*g*-PHBV behaved like a solid with a G' of about 5 kPa. This could be partially due to long chain branching between crosslinked PHBV (or PHB) chains. There was less of a magnitude increase in moduli for *α*Cell- PHB composites as compared to *α*Cell-PHBV due to grafting. This further indicated the higher grafted efficiency of PHBV based composites with incorporation of same peroxide concentration. The relatively lower degree of elasticity for PHB and PHBV compared with their composites was likely caused by their higher chain stiffness, and this phenomenon agrees with their higher T_m values. Therefore, peroxide induced free radical initiation to create crosslinks and grafting is a practical approach to improve the industrial melt processability of PHB and PHBV as well as their biocomposites.

3. Experimental

3.1. Materials

Lodgepole pine (*Pinus contorta*) lumber was sourced locally (Southern Idaho, USA). The lumber was chipped then Wiley-milled to pass through a 40 mesh screen. Wood fiber (500 g) was extracted with acetone (3 L, 99.5%, Macron Fine Chemicals) to yield 8.0 g of extractives. Air dried extractives free wood fiber (100 g batches) was treated with 3.2 L deionized water containing 30 g $NaClO_2$ (99%, Tech. Grade, Ricca Chemicals, USA) and acetic acid (20 mL, 99.7%, Fisher ACS, USA) at 70 ˚C for 1 h, and this was repeated four more times to a total of 6 h.[44] The holocellulose fibers (150 g batch) was then extracted with 17.5% NaOH (4 L) solution at 20 ˚C with constant stirring for 5 h to afford *α*Cell fibers by removing the hemicelluloses. The *α*Cell was recovered by filtering through a polypropylene screen (100 mesh) and washed

476 exhaustively with water under vacuum. Then, 10% aqueous acetic acid (2 L) was added to the
477 *α*Cell and left to soak for 5 min. The *α*Cell fiber was then washed exhaustively with water (1L,
478 10-15 times) until neutral. Finally, *α*Cell was rinsed with acetone to accelerate drying, and then
479 dried in a vacuum oven (>24 h) to <0.5% moisture content. This method yielded 55% *α*Cell
480 based on initial dry weight of wood.

481 Poly-3-hydroxybutyrate (PHB: M_w = 290,000 g/mol) and poly(3-hydroxybutyrate-co-3-
482 hydroxyvalerate) (PHBV: 22 mol% HV content; M_w = 400,000 g/mol) powder obtained from
483 Tianan Biopolymer Inc. (Ningbo, China). These PHAs are non-nucleated grades without any
484 additives. Dicumyl peroxide (DCP: 98%) was a product of Sigma-Aldrich (USA). CH_2Cl_2 (J.T.
485 Baker, USA) was used as received.

486

487 **3.2. Biocomposites processing**

488 The PHB and PHBV based composites were prepared according to our previous work.[26]
489 Briefly, *α*Cell, PHB and PHBV were separately coated with DCP in acetone solution (4-8
490 mg/mL) for 30 min, and then air dried followed by drying in a vacuum oven (>24 h) for prior to
491 composites processing. DCP coated PHB or PHBV (80%) and *α*Cell (20%; moisture content was
492 < 0.5%) were dried and premixed in a beaker. The *α*Cell-*g*-PHB and *α*Cell-*g*-PHBV grafted
493 biocomposites were prepared in a Dynisco Lab Mixer Molder/Extruder (LMM) using the
494 reactive extrusion process and mixed (500 rpm) for time t_R and then extruded into strands (1 mm
495 Ø) or injection molded into rectangular bars (60 x 9 x 2 mm^3). Processing temperature was 175
496 ˚C for PHB and 170 ˚C for PHBV based materials. The grafting efficiency (GE%) was evaluated
497 by extracting the non-soluble copolymerized gel fraction using Soxhlet extraction for 24 h in
498 chloroform to remove any nonreacted PHB. The extract was then filtered through a nylon screen

499 with pore size was about 450 μm which was large enough to allow nonreacted cellulose fibers to
500 pass through. The conditions (DCP concentration and reaction time t_R) at which maximum
501 grafted copolymer gel yield was considered to be optimized parameters used to prepare grafting
502 modified biocomposites.[19] Simple blends of *α*Cell and PHB (*α*Cell-PHB) or PHBV (*α*Cell-
503 PHBV) without addition of DCP were prepared as control strand and rectangular bar samples.
504

505 **3.3. Characterization**

506 3.3.1. *α*-Cellulose fiber analysis

507 Sieve analysis was performed on the isolated *α*Cell fibers (10 g) using standard test sieves
508 (40, 60, 80, 100, 200 mesh and pan) on a Soil Test Inc. Model CL-300B shaker for 10 min, and
509 the weight distribution was determined. The average length and diameters of the isolated *α*Cell
510 fibers in each fraction were averaged from two hundred fibers dyed with safranin and observed
511 by optical microscopy (Olympus BX51 in bright field mode and images captured using an
512 Olympus DP70 digital camera).

513 The chemical composition of the original wood and *α*Cell fibers for CH_2Cl_2 extractive,
514 lignin (acid soluble and Klason lignin), carbohydrate (hemicellulose and cellulose), and ash
515 compositions were determined according to the methods described in details by Liang and
516 McDonald.[45] More specifically, the wood and *α*Cell fibers samples (4-5 g) were Soxhlet
517 extracted with CH_2Cl_2 (150 mL) for 16 h in accordance with ASTM D 1108-9623 and
518 extractives were determined gravimetrically. Lignin content was determined as acid insoluble
519 and acid soluble lignin on extractive free samples. Carbohydrate analysis was performed on the
520 2-stage acid-hydrolyzates according to ASTM E 1758-01.26 with slight modification. The dried
521 sample (200 mg) was incubated in 72% H_2SO_4 (2 mL) for 1 h at 30 °C, then diluted into 4%

522 H_2SO_4, and subjected to secondary hydrolysis in an autoclave (117 KPa and 121 ˚C) for 30 min.
523 The hydrolyzate was filtered through a sintered crucible to obtain acid insoluble (Klason lignin)
524 residue content gravimetrically after oven dried at 104 ˚C. An aliquot of the hydrolysate (made
525 up to 250 mL) was taken to determine acid soluble lignin content at 205 nm using an absorption
526 coefficient of 110 L/g/cm on a Beckman DU640 spectrometer. To the hydrolysate (5 mL)
527 inositol (1 mL, 0.5 mg/mL) was added as an internal standard, then $PbCO_3$ (0.16 g) added to
528 remove sulfate, and centrifuged. The supernatant was deionized by passing through an ion
529 exchange resin cartridge (containing Amberlite IR-120 H^+ (0.5 mL) and Amberlite IRA35 OH^-
530 (0.5 mL)) and filtered through a 0.45 μm syringe filter (nylon, FisherScientific) into an HPLC
531 vial. Monosaccharides were quantified by HPLC using two Rezex RPM columns in series (7.8
532 mm × 30 cm, Phenomenex) at 85 ˚C equipped with a differential refractive index detector
533 (Waters Associates model 2414) on elution with water (0.5 mL/min). The chromatographic data
534 were analyzed using N2000 software (Science Technology Inc., China). The ash content of
535 lodgepole pine wood and isolated *α*Cell fibers were determined by furnacing samples at 600 ˚C
536 according to ASTM D 1102-84.
537
538 3.3.2. Surface morphology of composites
539 Biocomposite bar samples were microtomed into 100 μm thick specimens and coated with
540 carbon and gold. The prepared samples were investigated at 500x and 200x magnifications using
541 a LEO Gemini field emission SEM operating at 4 kV under high vacuum.
542
543 3.3.3. Surface chemistry by FTIR spectroscopy
544 *α*Cell fibers, PHB, PHBV, and biocomposites samples were characterized by FTIR

545 spectroscopy using a Thermo Nicolet iS5 FTIR spectrometer (ZnSe attenuated total reflection
546 (ATR) probe (iD5)). Samples (in triplicate) were analyzed after vacuum drying. The absorbance
547 spectra were baseline corrected and averaged using software Omnic v9.0 (Thermo Scientific).
548 Total crystallinity index (TCI) of *α*Cell fibers, and the quantitative crystallinity indices of
549 carbonyl (C=O stretching) group ($I_{C=O,\ PHB/PHBV}$) and C-O stretching ($I_{C-O,\ PHB/PHBV}$) of
550 PHB/PHBV polymers before and after grafting were determined as follows:

551 $$TCI = A_{1370}/A_{2900} \quad (3)$$

552 $$I_{C=O,\ PHB/PHBV} = A_{1720}/A_{1740} \quad (4)$$

553 $$I_{C-O,\ PHB/PHBV} = A_{1230}/A_{1450} \quad (5)$$

554 where A_{1370} and A_{2900} are the areas of *α*Cell peaks at 1370 and 2900 cm^{-1}, respectively, and
555 A_{1230}, A_{1450}, A_{1720} and A_{1740} are the areas of the peaks near to 1230, 1450, 1720 and 1740 cm^{-1}
556 from PHB (or PHBV) molecular chains, respectively. All band areas were obtained by peak
557 fitting processing using IGOR Pro v6 (WaveMetrics) software.[9] Gaussian functionality was
558 employed for peak fitting using selected peak width at half height (FWHM) values.
559
560 3.3.4. Crystallinity characterized by WAXD
561 The crystalline structures of *α*Cell fibers and injection molded neat PHB/PHBV and
562 biocomposites samples were characterized by WAXD (Siemens D5000 diffractometer) at room
563 temperature. The instrument was set up with a rotating Cu Kα2 X-ray tubes operating at 40 kV
564 with a current density of 30 mA. Scanning was performed over the 2θ ranging from 5 to 50° with
565 steps of 0.2°. The collected diffractograms were processed and peak of interest was
566 fitted/deconvoluted (Gaussian function) using IGOR Pro v6 software. The intensity of each peak
567 identified by peak fitting was mathematically computed. The methods to determine the

568 crystallinity index of αCell ($CrI_{\alpha Cell}$), PHB (CrI_{PHB}),[26] and PHBV (CrI_{PHBV}) are according to:

569 $$CrI_{\alpha Cell} = (1 - (I_{am}/I_{002})) \times 100 \quad (6)$$

570 where I_{am} is the intensity of the peak at $2\theta = 18°$ and I_{002} is the maximum intensity of the (002)

571 plane diffraction.

572 The PHB and PHBV crystallinity index was calculated according to:

573 $$CrI_{PHB} = I_{17}/I_{total\text{-}PHB} \times 100 \quad (7)$$

574 $$CrI_{PHBV} = I_{17}/I_{total\text{-}PHBV} \times 100 \quad (8)$$

575 where I_{17} is the intensity of the peak close to $2\theta = 17°$ and I_{total} is the total intensity of all

576 crystalline peaks of PHB ($I_{total\text{-}PHB}$) or PHBV ($I_{total\text{-}PHBV}$).

577 The crystal size dimension D_{hkl} was estimated as well by Scherrer's formula:[46]

578 $$D_{hkl} = K \times \lambda / (\beta_{1/2} \times \cos\theta) \quad (9)$$

579 where K is the crystal shape constant, λ is the X-ray wavelength ($\lambda = 0.1542$ nm, $\beta_{1/2}$ is the

580 FWHM, ≈ 2 Deg.) obtained by IGOR Pro, when peak fitting was conducted with Gaussian

581 function, and θ is the diffraction angle.

582

583 3.3.5. Tensile testing

584 All injection molded microtensile (dog-bone) samples (10 replicates) were conditioned at

585 65% relative humidity at 23 ˚C for at least 7 d. Tensile tests were performed according to ASTM

586 Standard D1708 using an Instron 5500R-1132 universal test machine with a constant strain rate

587 of 1 mm/min, 5 kN load cell, and strain measured using an extensometer (model 3542, Epsilon

588 Technology Corp.). The density of injection molded samples was calculated based on the initial

589 conditioned dry weight and dimensions.

590

3.3.6. Thermal analysis

TGA was performed on a TGA-7 (Perkin-Elmer) instrument. Samples (3-5 mg, in duplicates) were heated from 50 to 900 ˚C at a rate of 20 ˚C/min under nitrogen (30 mL/min). Data were analyzed with replicated curves were averaged using Pyris v8 software (Perkin Elmer).

DSC measurement was performed on neat PHB/PHBV and biocomposites (4-6 mg, in duplicate) using a TA Instruments model Q200 DSC with refrigerated cooling. The samples were (i) equilibrated at 40 ˚C (3 min) then ramped to 190 ˚C at 10 ˚C/min, held isothermally for 5 min to remove any thermal history, (ii) cooled to -50 ˚C at the rate of -10 ˚C/min and held isothermally for 3 min, and (iii) reheated to 190 ˚C at 10 ˚C/min to record the heating scan. Data were analyzed using TA Universal Analysis v4.4A software. Glass transition (T_g) and melting temperatures (T_m) were determined from the peaks second heating scan, while crystallization transition temperature (T_c) was obtained from the peak of cooling scan. The degree of crystallinity (X_c %) of PHB and PHBV was calculated as follows:

$$X_c\ \% = \Delta H_m/(\Delta H_0 \times W_f) \times 100 \qquad (10)$$

where ΔH_m is the melting enthalpy of sample (PHB and PHBV polymers), and ΔH_0 is melting enthalpy in J/g of 100% crystalline PHB (146 J/g),[37, 47] and W_f is the weight fraction of PHB or PHBV (80%) in biocomposites samples. Note: if the differences of transition temperatures between duplicates were less than 0.2 ˚C, standard deviation will not be reported.

DMA measurements were conducted on biocomposite samples using a TA Q800 Instruments. At least duplicate rectangular injection molded rectangular bars (60 x 9 x 2 mm^3) were tested using a 3-point bending fixture (50 mm span). Samples were heated from 30 to 150

˚C at 2 ˚C/min, 0.05% strain, and at a single frequency of 1 Hz. Data was analyzed by TA Universal Analysis v4.4A software.

The αCell/PHB and αCell/PHBV interfacial adhesion was evaluated by an adhesion factor (A) which was calculated from DMA results at 30 ˚C as follows:[9, 48]

$$A = (1/(1-V_f))\ (\tan \delta_c/\tan \delta_m) - 1 \quad (11)$$

where, c and m subscripts represent biocomposites and polymer matrix (PHB and PHBV), and V_f is the fiber volume fraction which was determined in accordance to ASTM standard D2584:

$$V_f = (W_f \rho_m)/(W_f \rho_m + W_m \rho_f) \quad (12)$$

where W_f is weight of αCell fibers which is 20%, W_m is the weight of polymer matrix which is 80%, ρ_f is the density of fibers (ρ_f = 1.5 g/cm^3),[49] and ρ_m is the density of matrix (ρ_m values of PHB and PHBV are 1.18 and 1.10 g/cm^3, respectively). V_f values of PHB and PHBV based composites were 16% and 15%, respectively.

3.3.7. Rheological analysis

The dynamic rheological measurements (G', G" and η*) were determined using a Bohlin CVO 100 rheometer, parallel plate (25 mm Ø), in oscillating shear mode with an ETC module on molded discs (2 mm x 25 mm Ø) samples. Experiments were performed in the linear viscoelastic region. For PHB and PHBV based materials, measurements were carried out at 175 and 170 ˚C, respectively, in the frequency range of 0.1 to 100 rad/s at an applied iso-strain of 0.5%. Data was analyzed using the Bohlin rheology v6.51 software.

4. Conclusion

The use of DCP in grafting modification of αCell/PHB and αCell/PHBV biocomposites via

637 *in-situ* reactive extrusion process was successful to achieve beneficial properties. Surface
638 morphology by SEM revealed better compatibility of cellulose in the polymer (PHB and PHBV)
639 matrix of the resultant biocomposites due to grafting modification as compared to blends. The
640 tensile tests showed the grafting increased the toughness and flexibility of biocomposites due to
641 the enhanced fiber-polymer matrix interaction and lower degree of crystallinity as compared to
642 neat polymers and simple blends. The degree of crystallinity of the composites was reduced
643 through grafting, which was reflected by the crystallinity indices estimated from quantitative
644 FTIR and WAXD analyses. Grafting was found to have a significant influence on the thermal
645 properties (e.g. stability) of *α*Cell-*g*-PHB/PHBV biocomposites. Lower processing temperatures
646 and shorter cycle times during melt processing could be achieved and further minimize
647 degradation. Grafting improved the interfacial bonding between *α*Cell fibers and polymer matrix
648 as determined by the adhesion factor. It can be concluded that this approach afforded cellulose
649 reinforced bioplastic composite materials with significantly improved mechanical and thermal
650 properties by chemically grafting the fibers with the matrix to improve stress transfer. This
651 grafting modification was achieved via a one-step reactive extrusion process and can provide a
652 sustainable strategy to utilize cellulose fibers derived from various renewable resources
653 including any at-risk intermountain wood species to create value added products. This developed
654 technique can be applied to PHB/PHBV biosynthesized from waste substrate by mixed microbial
655 consortia to lower the cost of these materials which will help their applications as bulk materials.

656 # Acknowledgement

657 The authors would like to acknowledge (i) the financial support from a USDA-Forest
658 Products Laboratory Grant 08-JV-111111, (ii) USDA-CSREES Grant 2007-34158-17640 for
659 supporting the DSC and DMA, and (iii) ThermoScientific for the FTIR spectrometer.

References

1. G.-Q. Chen and M. K. Patel, *Chem. Rev.*, 2012, **112**, 2082-2099.

2. R. U. Halden, *Annual Review of Public Health*, 2010, **31**, 179-194.

3. D. Garlotta, *J. Polym. Environ.*, 2001, **9**, 63-84.

4. T. Mekonnen, P. Mussone, H. Khalil and D. Bressler, *Journal of Materials Chemistry A*, 2013, **1**, 13379.

5. J. Lunt, *Polym. Degrad. Stab.*, 1998, **59**, 145-152.

6. M. Yamaguchi and K. Arakawa, *Eur. Polym. J.*, 2006, **42**, 1479-1486.

7. R. M. Rasal, A. V. Janorkar and D. E. Hirt, *Prog. Polym. Sci.*, 2010, **35**, 338-356.

8. A. Youngblood, J. Zhu and C. T. Scott, presented in part at the National Silviculture Workshop, Boise, Idaho, 15–18 June, 2009.

9. L. Wei, A. G. McDonald, C. Freitag and J. J. Morrell, *Polym. Degrad. Stab.*, 2013, **98**, 1348-1361.

10. K. Suzuki, A. Sato, H. Okumura, T. Hashimoto, A. N. Nakagaito and H. Yano, *Cellulose*, 2013, **21**, 507-518.

11. C. Fonseca-Valero, A. Ochoa-Mendoza, J. Arranz-Andrés and C. González-Sánchez, *Composites Part A*, 2015, **69**, 94-104.

12. M. Pöllänen, M. Suvanto and T. T. Pakkanen, *Compos. Sci. Technol.*, 2013, **76**, 21-28.

13. A. K. Bledzki and J. Gassan, *Prog. Polym. Sci.*, 1999, **24**, 221-274.

14. M. Bengtsson, P. Gatenholm and K. Oksman, *Compos. Sci. Technol.*, 2005, **65**, 1468-1479.

15. L. C. Tomé, R. J. B. Pinto, E. Trovatti, C. S. R. Freire, A. J. D. Silvestre, C. P. Neto and A. Gandini, *Green Chem.*, 2011, **13**, 419.

16. A. Gandini, *Green Chem.*, 2011, **13**, 1061.

17. O. Faruk, A. K. Bledzki, H.-P. Fink and M. Sain, *Prog. Polym. Sci.*, 2012, **37**, 1552-1596.

18. M. John and S. Thomas, *Carbohydr. Polym.*, 2008, **71**, 343-364.

19. D. Roy, M. Semsarilar, J. T. Guthrie and S. Perrier, *Chem. Soc. Rev.*, 2009, **38**, 2046-2064.

689 20. L. Yu, K. Dean and L. Li, *Prog. Polym. Sci.*, 2006, **31**, 576-602.

690 21. S. A. Madbouly, J. A. Schrader, G. Srinivasan, K. Liu, K. G. McCabe, D. Grewell, W. R.
691 Graves and M. R. Kessler, *Green Chem.*, 2014, **16**, 1911.

692 22. L. Wei, S. Liang and A. G. McDonald, *Ind. Crop. Prod.*, 2015, **69**, 91–103.

693 23. D. Roy, M. Semsarilar, J. T. Guthrie and S. Perrier, *Chem. Soc. Rev.*, 2009, **38**, 2046-
694 2064.

695 24. A. Carlmark, E. Larsson and E. Malmström, *Eur. Polym. J.*, 2012, **48**, 1646-1659.

696 25. N. Le Moigne, M. Longerey, J.-M. Taulemesse, J.-C. Bénézet and A. Bergeret, *Ind.*
697 *Crop. Prod.*, 2014, **52**, 481-494.

698 26. L. Wei, A. G. McDonald and N. M. Stark, *Biomacromolecules*, 2015, **16**, 1040–1049.

699 27. T. A. Clark, K. L. Mackie, P. H. Dare and A. G. McDonald, *J. Wood Chem. Technol.*,
700 1989, **9**, 135-166.

701 28. J. Yang, J.-J. Zhao, F. Xu and R.-C. Sun, *ACS Appl. Mater. Interfaces*, 2013, **5**, 12960-
702 12967.

703 29. K. Joseph and S. Thomas, *Polymer*, 1996, **37**, 5139-5149.

704 30. W. J. Orts, R. H. Marchessault, T. L. Bluhm and G. K. Hamer, *Macromolecules*, 1990,
705 **23**, 5368-5370.

706 31. K. Sudesh, H. Abe and Y. Doi, *Prog. Polym. Sci.*, 2000, **25**, 1503-1555.

707 32. L. Wei, N. M. Guho, E. R. Coats and A. G. McDonald, *J. Appl. Polym. Sci.*, 2014, **131,**
708 **40333, doi: 10.1002/app.40333**.

709 33. D. Maldas and B. V. Kokta, *J. Adhes. Sci. Technol.*, 1994, **8**, 1439-1451.

710 34. N. M. Barkoula, S. K. Garkhail and T. Peijs, *Ind. Crop. Prod.*, 2010, **31**, 34-42.

711 35. M. Avella, G. La Rota, E. Martuscelli and M. Raimo, *J. Mater. Sci.*, 2000, **35**, 829-836.

712 36. S. Modi, K. Koelling and Y. Vodovotz, *Eur. Polym. J.*, 2011, **47**, 179-186.

713 37. L. Wei and A. G. McDonald, *J. Appl. Polym. Sci.*, 2015, **132, Doi: 10.1002/app.41724**.

714 38. R. Bhardwaj, A. K. Mohanty, L. T. Drzal, F. Pourboghrat and M. Misra,
715 *Biomacromolecules*, 2006, **7**, 2044-2051.

716 39. M. Scandola, M. L. Focarete, G. Adamus, W. Sikorska, I. Baranowska, S. Swierczek, M.
717 Gnatowski, M. Kowalczuk and Z. Jedlinski, *Macromolecules*, 1997, **30**, 2568-2574.

40. J. O. Zoppe, M. S. Peresin, Y. Habibi, R. A. Venditti and O. J. Rojas, *ACS Appl. Mater. Interfaces*, 2009, **1**, 1996-2004.

41. E. Ten, D. F. Bahr, B. Li, L. Jiang and M. P. Wolcott, *Ind. Eng. Chem. Res.*, 2012, **51**, 2941-2951.

42. D. Yan, W.-J. Wang and S. Zhu, *Polymer*, 1999, **40**, 1737-1744.

43. D. H. S. Ramkumar and M. Bhatacharya, *Polym. Eng. Sci.*, 1998, **38**, 1426-1435.

44. J. S. Fabiyi, A. G. McDonald, M. P. Wolcott and P. R. Griffiths, *Polym. Degrad. Stab.*, 2008, **93**, 1405-1414.

45. S. Liang and A. G. McDonald, *J. Agric. Food Chem.*, 2014, 140805102128006.

46. L. E. Alexander, *X-ray diffraction method in polymer science*, Wiley-Interscience, New York, 1969.

47. P. J. Barham, A. Keller and E. L. Otun, *J. Mater. Sci.*, 1984, **19**, 2781-2794.

48. J. Kubát, M. Rigdahl and M. Welander, *J. Appl. Polym. Sci.*, 1990, **39**, 1527–1539.

49. W. A. Sisson, in *Cellulose and cellulose derivatives*, ed. E. Ott, Interscience, New York., 1943, ch. 4, pp. 214, vol. 5, ch. 3.

736 **Table 1** Chemical composition of the lodgepole pine wood and isolated *α*Cell fibers (dry basis).

Composition	Lodgepole pine wood (%)	*α*-Cellulose (%)
Cellulose	39.1	95.9
Glucan 6C	39.1	95.9
Hemicellulose	33.1	3.9
Xylan 5C	5.3	3.8
Galactan 6C	11.5	0.0
Mannan 6C	16.3	0.1
Arabinan 5C	1.5	0.0
Lignin	26.9	0.2
Klason lignin	26.5	0.2
Acid soluble lignin (ASL)	0.4	0.0
CH_2Cl_2 extractives	1.7	0.0
Ash	0.01	0.0

737

738 **Table 2** Yield of each fraction of *α*Cell fibers retained on sieves with various openings, and the
739 averaged fiber length, diameter, and the aspect ratio measured by microscopic analysis.

Retained on mesh	Sieve opening (μm)	Particle weight fraction (%)	Fiber length (L, mm)[b]	Fiber diameter (d, μm)[a]	Aspect ratio (L/d)
40	420	7.3	-	-	-
60	250	6.3	-	-	-
80	177	16.0	0.8 ± 0.1	19.0 ± 1.6	42.1
100	149	11.4	0.7 ± 0.1	18.7 ± 2.8	37.4
200	70	37.5	0.6 ± 0.1	18.5 ± 2.0	32.4
< 200	<70	21.5	0.4 ± 0.1	14.0 ± 2.1	28.6
Average			0.5	15.1	29.3

740 [a] The fiber length and diameter of *α*Cell fibers of the 60 and 40 mesh fractions could not be
741 accurately determined due to fiber bundles as shown in Fig. 2a and 2b.
742

743 **Table 3** Crystallinity parameters characterized by FTIR and WAXD. [a]

Sample	FTIR			WAXD			
	$TCI_{\alpha Cell}$	$I_{C=O,\ PHB/PHBV}$	$I_{C-O,\ PHB/PHBV}$	$CrI\%_{\alpha Cell}$	$CrI\%_{PHB/PHBV}$	D (002) (Å)	D (020) (Å)
*α*Cell	0.4	-	-	59.1	-	250	-
PHB	-	3.8	2.0	-	61.0	-	1274
*α*Cell-PHB	0.3	3.3	0.6	56.4	57.9	233	1108
*α*Cell-*g*-PHB	0.1	2.2	0.4	33.9	45.4	90	312
PHBV	-	2.7	0.8	-	36.2	90	190
*α*Cell-PHBV	0.3	2.6	0.4	40.2	34.2	82	153
*α*Cell-*g*-PHBV	0.1	1.8	0.1	28.7	26.4	40	97

744 [a] Crystal sizes were determined in the direction perpendicular to the planes of (002) and (020) for

745 *α*Cell and polymers PHB and PHBV, respectively.

Table 4 Density (ρ), tensile strength (σ), tensile (Young's) modulus (E), elongation at break (ε), and energy at break (EAB) of molded neat PHB/PHBV and their biocomposites samples (10 replicates). Standard deviation values are given in parentheses. Samples with same letter are not significantly different at 95% confidence interval of probability using Tukey's paired t-tests.

Sample	ρ (g/cm^3)	E (GPa)	σ (MPa)	ε (%)	EAB (J)
Neat PHB	1.18 (0.02)^{abc}	2.2 (0.3)^{a}	23.1 (3.3)^{a}	13.6 (1.0)^{a}	0.33 (0.03)^{a}
αCell-PHB	1.14 (0.03)^{abc}	2.6 (0.2)^{ab}	25.9 (1.4)^{ab}	11.2 (0.3)^{b}	0.41 (0.03)^{b}
αCell-*g*-PHB	1.10 (0.02)^{abc}	5.5 (0.7)^{c}	28.1 (1.8)^{c}	13.2 (2.0)^{ac}	0.60 (0.05)^{c}
Neat PHBV	1.18 (0.01)^{def}	0.9 (0.1)^{d}	11.8 (2.0)^{d}	19.6 (1.8)^{d}	0.45 (0.03)^{d}
αCell-PHBV	1.10 (0.02)^{def}	1.3 (0.1)^{e}	13.9 (2.5)^{e}	15.4 (1.8)^{e}	0.53 (0.05)^{e}
αCell-*g*-PHBV	1.06 (0.02)^{def}	2.4 (0.3)^{f}	15.9 (1.7)^{f}	18.8 (1.0)^{df}	0.76 (0.05)^{f}

752 **Table 5** Thermal degradation temperatures of PHB and PHBV based biocomposites obtained

753 from TGA data. [a]

Samples	T_{onset} (˚C)	T_{max} (˚C)		T_{comp} (˚C)
		T_{PHB}/T_{PHBV} (˚C)	$T_{\alpha Cell}$ (˚C)	
α-Cellulose	303		342	400
PHB	263	285		303
*α*Cell-PHB	264	287	328	358
*α*Cell-*g*-PHB	277	298	335	364
PHBV	250	270		292
*α*Cell-PHBV	253	273	334	362
*α*Cell-*g*-PHBV	260	284	340	363

754 [a] T_{onset} = beginning weight loss; T_{max} = the temperature of maximum decomposition rate; T_{PHB},

755 T_{PHBV} = maximum decomposition rate of PHB and PHBV degradation stage (the 1st stage of

756 biocomposites), respectively; $T_{\alpha Cell}$ = maximum decomposition rate of *α*Cell degradation (the 2nd

757 stage of biocomposites); T_{comp} = 100% mass loss onset point.

758

Table 6 Crystallization temperature (T_c), peak temperatures of the low- and high-temperature endotherms (T_{m1} and T_{m2}), and degree of crystallinity (X_c %). Standard deviation values are given in parentheses.

Samples	T_g (˚C)	T_{m1}(˚C)	T_{m2} (˚C)	X_c (%)	T_c (˚C)	T_c (˚C)	ΔH_c (J/g)
Neat PHB	4.9	159	169	53.4 (1.2)	85	ND	67
*α*Cell-PHB	5.3	161	171	50.0 (0.5)	121	ND	63
*α*Cell-*g*-PHB	6.9	155	164	43.0 (2.3)	103	ND	55
Neat PHBV	-4.0	129	153	17.8 (0.5)	67	ND	27
*α*Cell-PHBV	-2.0	126	151	16.8 (1.1)	39	56.4	22
*α*Cell-*g*-PHBV	-0.5	118	135	4.60 (0.2)	ND	76.5	ND

ND: not detected.

Table 7 Comparative storage moduli (E') at selected temperatures, tanδ and adhesion factor (A) near to room temperature (30 ˚C) of neat PHB and PHBV based samples. Standard deviation values are given in parentheses.

Samples	Storage modulus E' (MPa)			Tanδ			V_f(%)	$A_{30°C}$
	30 ˚C	50 ˚C	70 ˚C	Tan$\delta_{30\ °C}$	Tan$\delta_{50\ °C}$	Tan$\delta_{70\ °C}$		
Neat PHB	1797	1466	1276	0.076	0.037	0.040	0	-
αCell-PHB	2395	2073	1820	0.070	0.043	0.050	16 (0.5)	1.25 (0.20)
αCell-*g*-PHB	2869	2255	1934	0.040	0.035	0.054	15 (1.2)	0.28 (0.00)
Neat PHBV	630	548	439	0.090	0.065	0.074	0	-
αCell-PHBV	1182	742	486	0.065	0.068	0.090	16 (0.5)	0.72 (0.14)
αCell-*g*-PHBV	1432	985	706	0.050	0.080	0.104	15 (1.2)	0.32 (0.02)

Note: the differences of moduli and Tanδ between duplicates were less than 20 MPa and 0.005, respectively; hence standard deviation was not reported.

769

770 **Fig. 1.** Generalized schematic representation of grafted PHB or PHBV polymers onto *α*Cell (a),

771 and the chemical structures of grafted *α*Cell-*g*-PHB (b) and *α*Cell-*g*-PHBV (c) biocomposites.

772

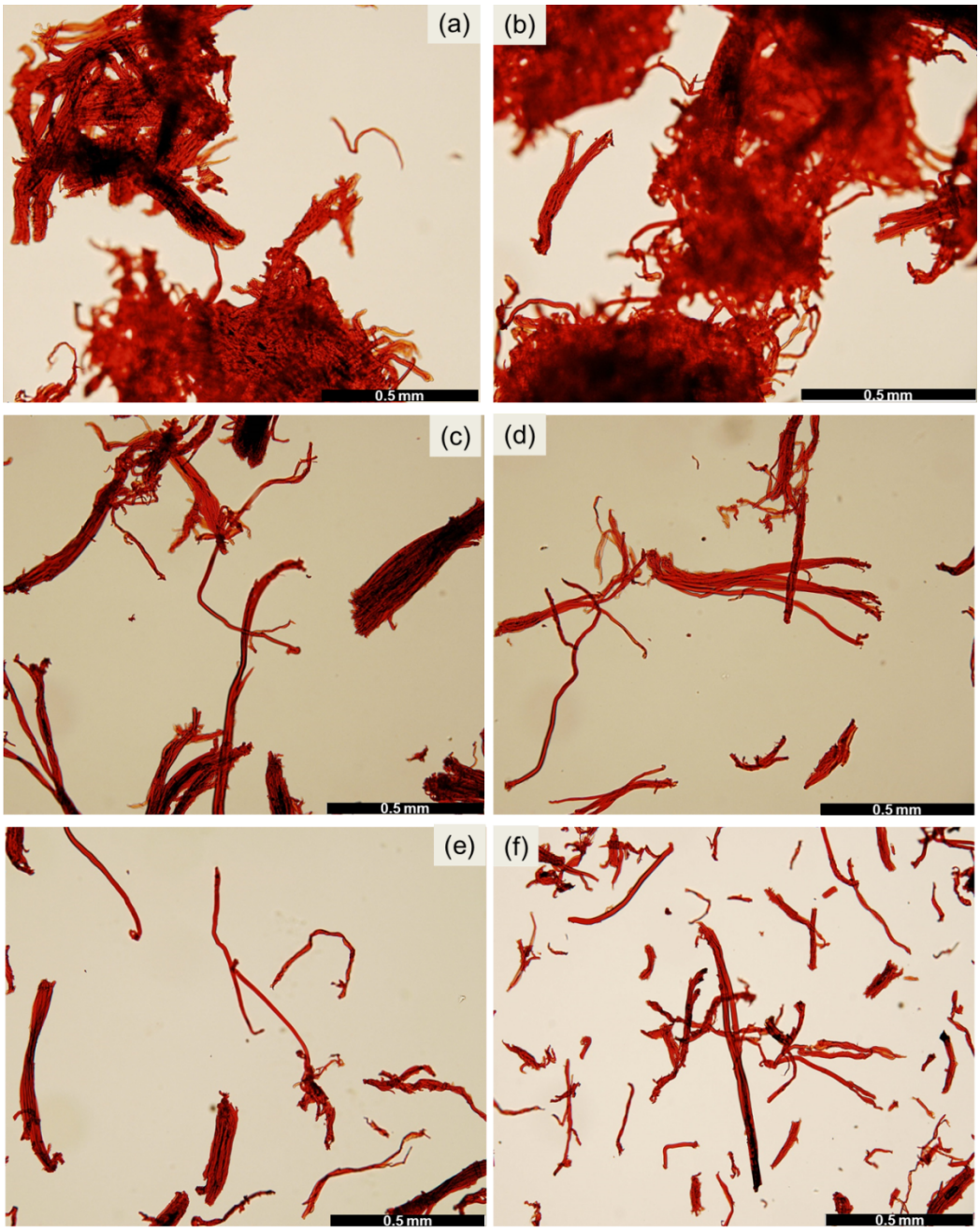

773

774 **Fig. 2** Optical micrographs of *α*Cell fibers fractions classified (a) >40 mesh, (b) >60 mesh, (c)

775 >80 mesh, (d) >100 mesh, (e) >200 mesh and (d) <200 mesh.

776

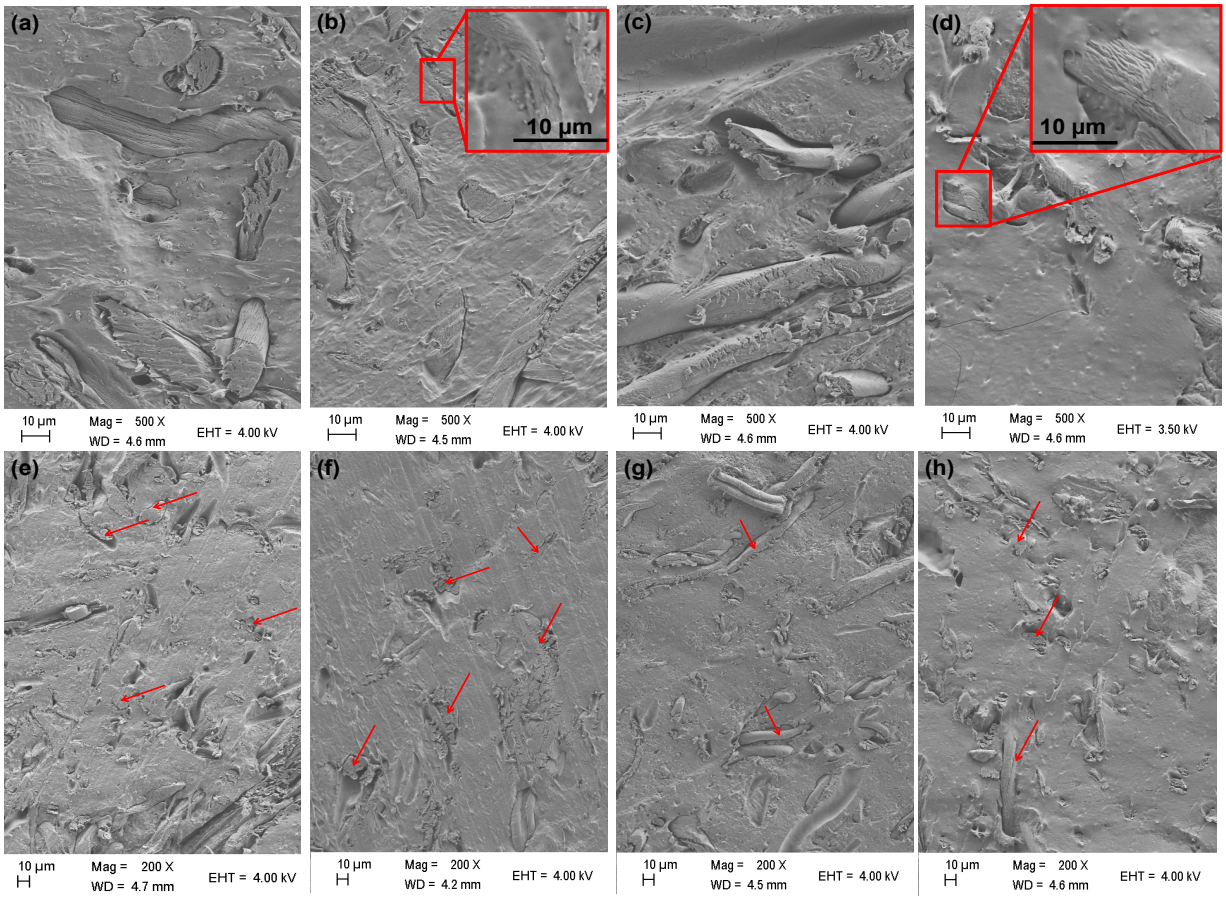

Fig. 3 SEM micrographs of surface morphologies of *α*Cell-PHB (a: 500x; e: 200x), *α*Cell-*g*-PHB (b: 500x; f: 200x), *α*Cell-PHBV (c: 500x; g: 200x), and *α*Cell-*g*-PHBV (d: 500x; h: 200x) composites. Note: fiber and polymer matrix interface was shown in in-set micrographs with larger magnification (1000x) of the grafted composites (b and d); fibers are pointed out by arrows.

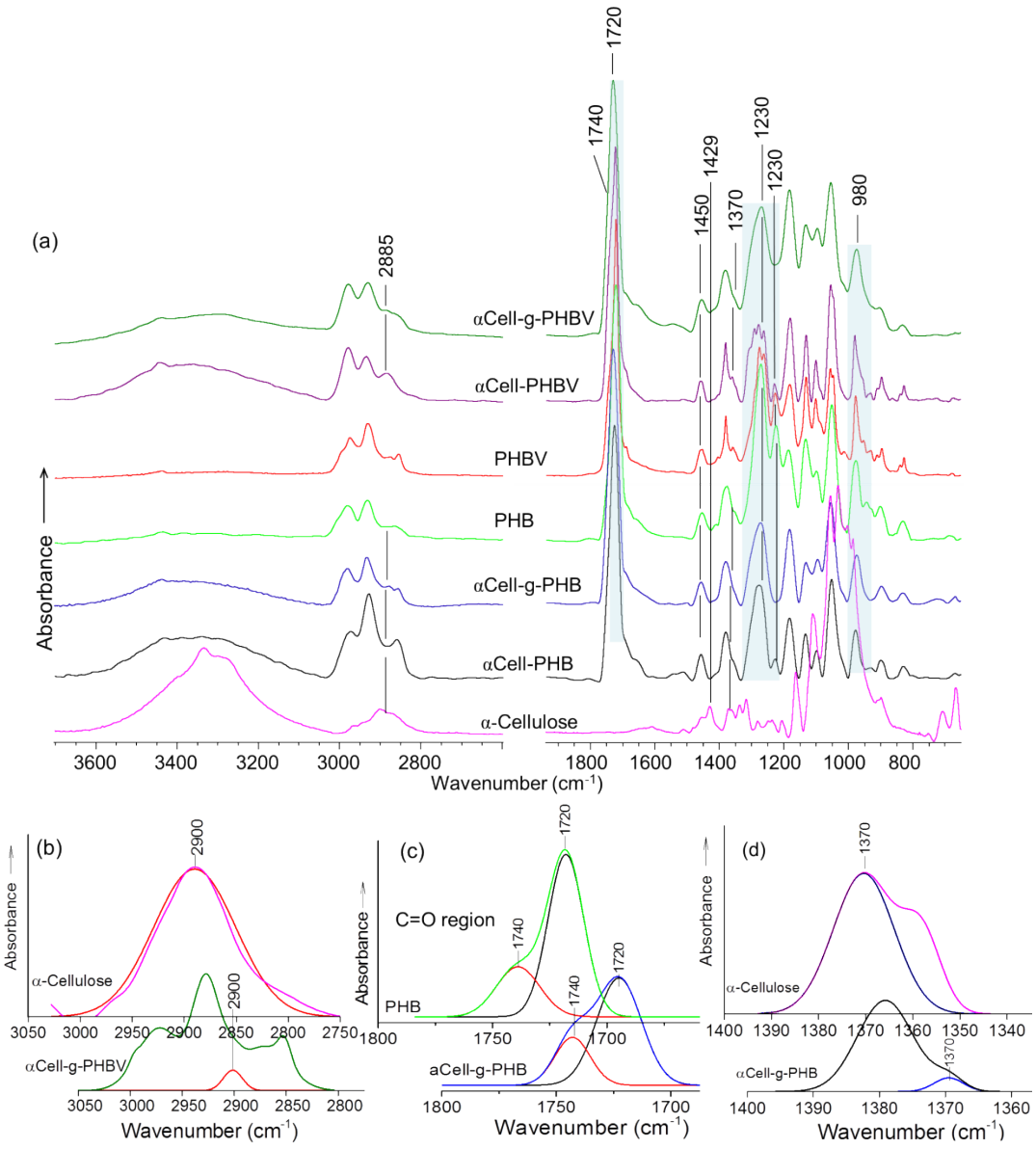

785

786 **Fig. 4** (a) FTIR spectra for *α*-cellulose, PHB, PHBV, and their composites samples; (b) –C–H

787 stretching (2900 cm^{-1}) fitted bands for *α*Cell and *α*Cell-*g*-PHBV composites; (c) carbonyl (C=O)

788 fitted peaks for PHB and *α*Cell-*g*-PHB composite, and (d) –C–H bending (1370 cm^{-1}) fitted

789 peaks for *α*Cell and *α*Cell-*g*-PHB composite.

790

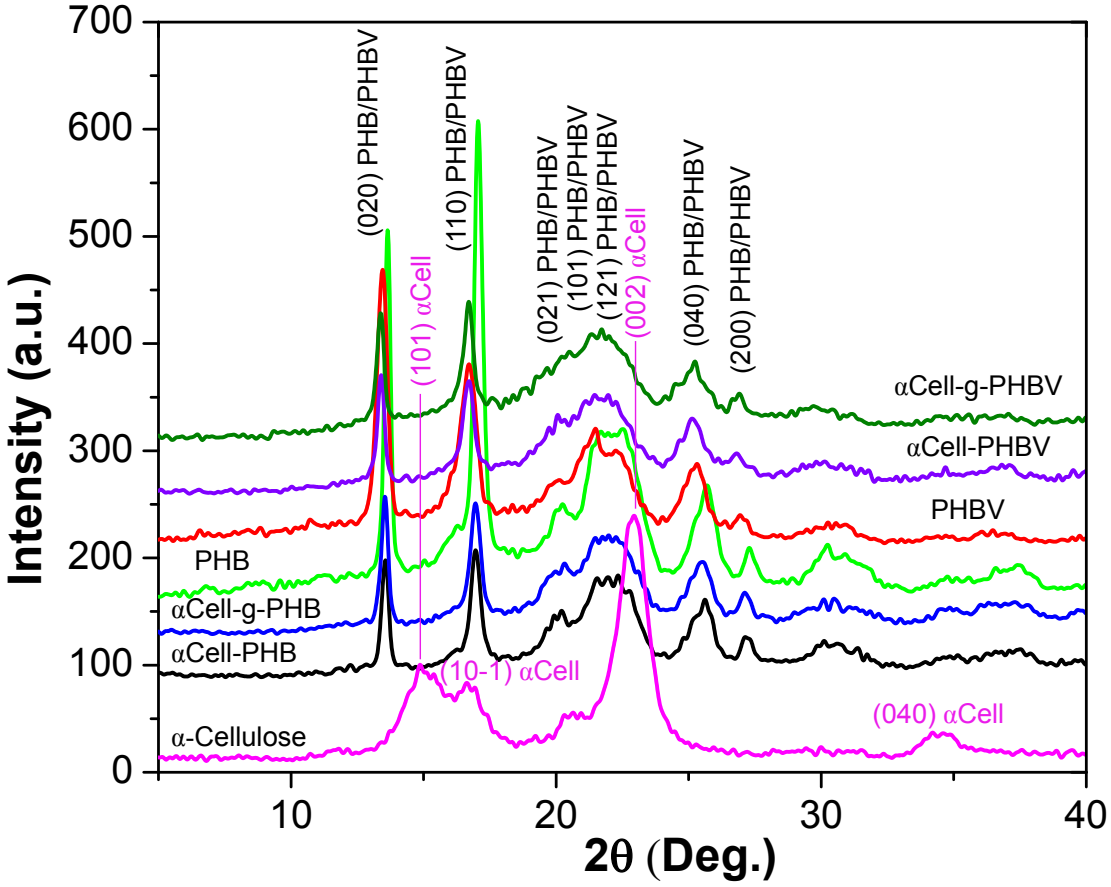

791

792 **Fig. 5** XRD diffractograms of *α*Cell, PHB, PHBV, blended composite (*α*Cell-PHB and *α*Cell-

793 PHBV) and grafted composite (*α*Cell-*g*-PHB and *α*Cell-*g*-PHBV) samples.

794

795

796 **Fig. 6** DSC cooling and the 2nd heating curves of (a) PHB, *α*Cell-PHB and *α*Cell-*g*-PHB and (b)

797 PHBV, *α*Cell-PHBV and *α*Cell-*g*-PHBV samples.

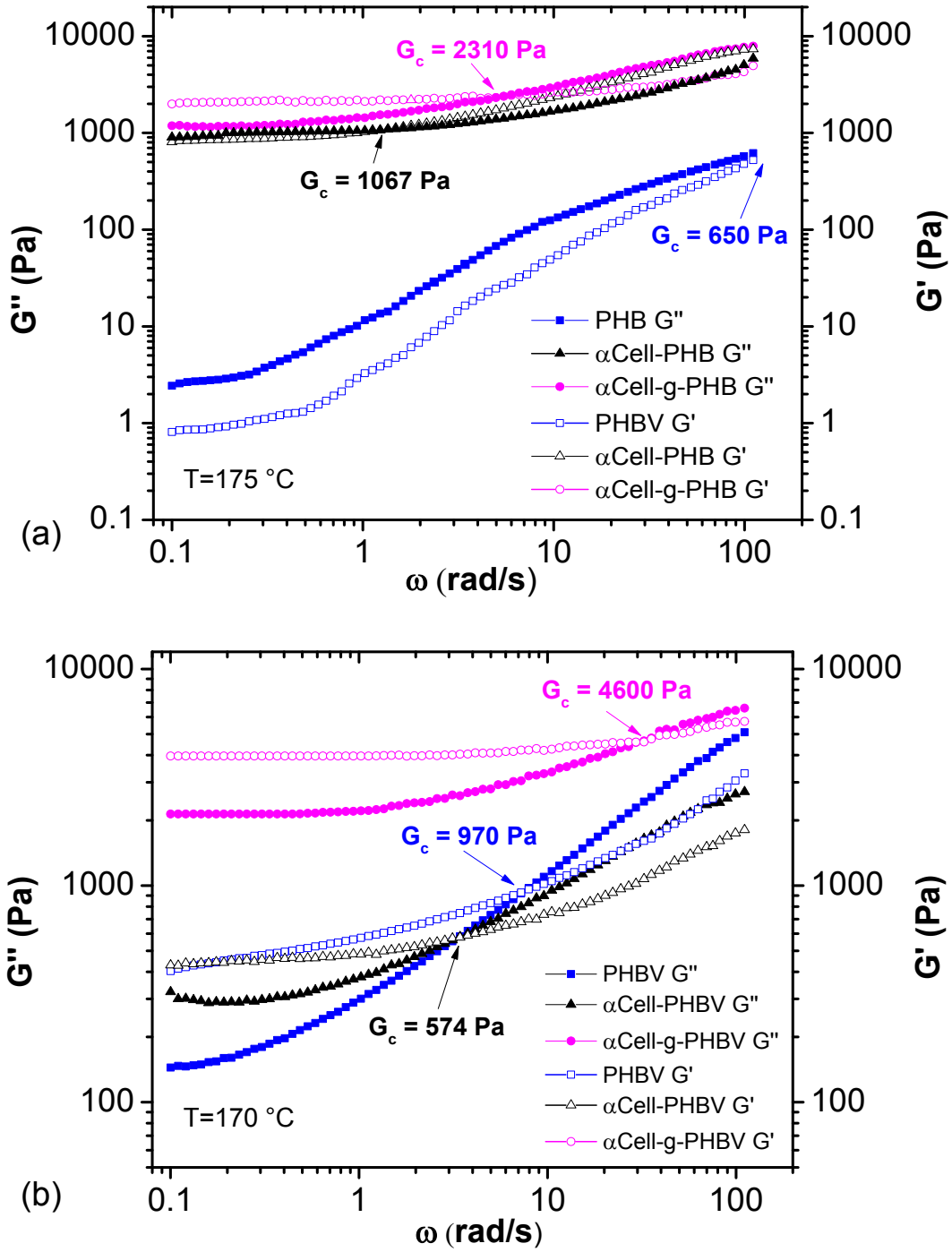

798

799 **Fig. 7** Effect of grafting on dynamic rheology storage (G') and loss (G") moduli of (a) PHB,

800 *α*Cell-PHB, and *α*Cell-g-PHB samples at 175 ˚C and (b) PHBV, *α*Cell-PHBV and *α*Cell-g-PHBV

801 samples at 170 ˚C. G_c is the crossover modulus when G' = G".

802